

# Microstructure-Property Relationships in HAZ of New 13% Cr Martensitic Stainless Steels

*An assessment of mechanical properties showed a relatively low HAZ hardness and high notch toughness could be obtained*

BY O. M. AKSELSEN, G. RØRVIK, P. E. KVAALE, AND C. VAN DER EIJK

**ABSTRACT.** In the present investigation, the properties of new low-carbon (0.01–0.1 wt-% C), 13 wt-% chromium, martensitic stainless steels have been examined. The major focus has been put on an assessment of the mechanical properties of weld simulated specimens, including Charpy V-notch (CVN) toughness and tensile properties. The steels included are different types of martensitic grades, ranging from the “old, conventional” type with 0.1% C to the new low-carbon (< 0.02% C) steels with balanced additions of Cr, Ni, and Mo to improve corrosion resistance and to maintain phase balance.

The results showed that a relatively low heat-affected zone hardness ( $HV_5 < 300$  kg/mm<sup>2</sup>) can be obtained, depending on the steel’s chemical composition, weld simulation parameters, and the application of a tempering cycle. Single values as low as about 270 kg/mm<sup>2</sup> have been achieved for the lowest carbon-containing steels. The notch toughness, which is of primary concern, was quite high (> 50 joules), with the exception of the steel with the highest carbon content (0.11% C). After a tempering pulse (600°, 700°, and 800°C for 60 s), the steels behave quite differently. While hardness was reduced for most of the steels, toughness was reduced for one of the steels and improved for two of them, and with some embrittlement phenomenon for two of them. The low-carbon, high-alloy-type steel E with 12Cr-6Ni-2.5Mo, and the lean alloy-type steel A with 13Cr-4.7Ni-1.7Mo appeared to have the best overall notch toughness after short pulse tempering. The compositions of these two steels are very close to those now commercially available.

## Introduction

### Background

At present, the 13% Cr martensitic stainless steels have been used in many sub-

O. M. AKSELSEN and C. VAN DER EIJK are with SINTEF, Trondheim, Norway. G. RØRVIK and P. E. KVAALE are with Statoil Research Center, Trondheim, Norway.

sea production systems and satellite fields, e.g., *Haltenbanken* and *Gullfaks* fields at the Norwegian continental shelf (Refs. 1–3). These are connected to production platforms through interfield flowlines with outer diameters between 8 and 12 in. (~203–305 mm), only a few lines are in the range of 16 to 24 in. (~406–610 mm) diameter. The martensitic 13% Cr class of stainless steels has been regarded as a possible material candidate due to its very high potential for cost savings compared with the more familiar duplex grades. The present investigation was, therefore, carried out as part of a larger qualification of the 13% Cr steel class. The investigation is based on a study of the relationship between the weld thermal program (cooling rate, peak temperature, subsequent tempering) and heat-affected zone (HAZ) mechanical properties (Charpy V-notch toughness, tensile strength and ductility, hardness), using the weld simulation technique. A wide range of martensitic steels is included, ranging from the “older” class with relatively high carbon content (~0.1% C) and no alloying with the exception of Cr, to the new so-called “supermartensitic” grades with improved weldability, based upon low carbon (< 0.02%) content and balanced additions of alloying elements such as Ni and Mo to improve the corrosion properties and to maintain the microstructural balance.

### Transformation Behavior of Martensitic Stainless Steels

The peak temperature corresponds to a certain point within the HAZ, which can be divided into six separate regions according to the Fe-Cr-Ni phase diagram shown in Fig. 1 (Refs. 4–6). The tempera-

ture range of stability for the different phases is also outlined in Table 1, and can be defined as follows under heating of the base metal up to the melting point:

1) Subcritical/tempered region, where no transformation takes place (below  $A_{c1}$ ), but with possible carbide precipitation.

2) Low-temperature, two-phase region with austenite and ferrite ( $\gamma + \alpha$ ), between 460°–600° and 630°–700°C.

3) Single-phase austenite region, with the temperature range from about 630°–720°C to about 1200°–1260°C, though strongly dependent on the steel composition.

4) High-temperature, two-phase region with a mixture of delta ferrite and austenite ( $\delta + \gamma$ ), within the temperature range between 1200°–1260° and 1310°–1390°C, depending on the actual chemical composition.

5) Single-phase  $\delta$  ferrite region, within the temperature range between 1310°–1390° and 1440°C.

6) Partially melted region, within the temperature range between 1440° and 1470°C.

It is important to point out that the existence regime of the different regions is strongly dependent on the steel’s chemical composition. In addition, the heating rate is important, and substantial superheating may be required compared with the Fe-Cr-Ni alloy equilibrium diagram in Fig. 1.

Supermartensitic steels are normally divided into three types, i.e., lean (11Cr-2Ni), medium (12Cr-4.5Ni-1.5Mo) and high alloyed grades (12Cr-6Ni-2.5Mo) (Refs. 7, 8). In the present investigation, all grades are included, in addition to two Cr (11% and 13% Cr) steels with low Ni (0.8% and 0.5% Ni), but with no Mo. One of these contains high carbon (0.11%), as the representative of the “old, traditional” martensitic stainless steels.

## Materials and Experimental Procedure

### Materials

Five martensitic stainless steels have been included in the present study. Their

### KEYWORDS

Martensitic Stainless Steels  
13% Cr Steels  
HAZ Properties  
Weld Simulations  
Tempering  
Supermartensitic Steels  
Pipeline Steels  
Weld Toughness

chemical composition and mechanical properties are outlined in Tables 2 and 3, respectively. Table 2 reveals that there are relatively large differences between the steels when it comes to the contents of C, Mn, Cu, Ni, Cr, Mo, and N. This may, in turn, influence the transformation behavior and, hence, the mechanical properties. The position of the different steels in the Schaeffler diagram is indicated in Fig. 2, and implies that most of the steels (B, C, and E) fall within the martensite-rich region of the two-phase martensite-ferrite regime. Steel A contains a mixture of martensite and ferrite stringers, possibly with retained austenite, which is not readily visible in the light microscope. Steel D falls within the martensite region. The different base metal microstructures are exemplified by the micrographs of steels A and D in Fig. 3.

Table 3 shows that the strength of the selected steels is relatively high, particularly for steel A, with yield and tensile strengths of 619–762 and 915–950 MPa, respectively. Modern supermartensitic steels are now made to satisfy requirements set to the X80 pipeline grade (Ref. 8).

### Weld Simulation

The weld simulation experiments were carried out by two different techniques:

1) Resistance heating of specimens with  $10.5 \times 10.5 \text{ mm}^2$  cross section and 100 mm length for subsequent Charpy V-notch (CVN) testing

2) Induction heating of specimens with 10–12 mm diameter and 100 mm length for subsequent tensile testing.

The investigation included weld simulation with different peak temperatures,  $T_p$ , and cooling times between 800° and 500°C,  $\Delta t_{8/5}$ . The heating rate was 200°C/s. In addition, the potential effects of tempering pulses were examined using a first weld cycle with  $T_p$  of 1350°C followed by a second tempering cycle with various peak temperatures and holding times. In this case, the heating rate in the first and second cycle was 200° and 50°C/s, respectively. The cooling rate during the tempering pulse was 20°C/s. In spite of the lower heating rate in the case of tempering pulses, some overheating (between 15° and 20°C) occurred before the temperature was sta-

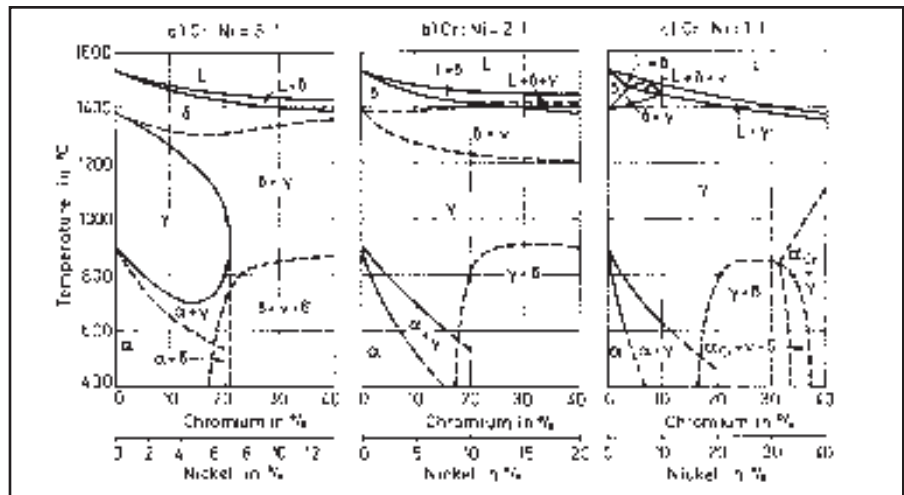


Fig. 1 — The Fe-Ni binary phase diagram, with 12% Cr /4/.

bilized (after 3–5 s) at the preprogrammed level. The associated phase transformation temperatures were recorded by dilatation, including the  $A_{c1}$  and  $A_{c3}$  temperatures during heating and the  $M_s$  and  $M_f$  temperatures during cooling.

Assessment of the HAZ strength and ductility was done, as indicated above, on the basis of tensile testing of weld simulated specimens. Bars of 8 mm diameter and 70 mm length were heated by induction to various peak temperatures, followed by controlled cooling in helium. Originally, a peak temperature of 1350°C was desired, but this was reduced to 1250°C, since partial melting occurred. In

spite of the reduced peak temperature, the austenite grain size is large due to the very slow heating rate obtained through the high-temperature range (> the Curie temperature, i.e., > about 670°C). By contrast, the heating rate is rapid until the Curie temperature is reached. The cooling time,  $\Delta t_{8/5}$ , was adjusted to 12 s. The temperature-time cycles were recorded by chromel/alumel thermocouples spot welded at the midlength of the bar surface. Due to the small bar dimensions involved, specimens exhibited a uniform microstructure and hardness over the entire specimen length and cross section after weld simulation.

Table 1 — Phase Stability in the HAZ of Fe-Cr-Ni Alloys

Phase	Temperature Range		HAZ Region
	Cr:Ni = 3:1	Cr:Ni = 2:1	
$\alpha[\alpha']$	RT–~600°C	RT–~460°C	Subcritical region
$\alpha + \gamma$	~600°–~710°C	~460°–~630°C	
$\gamma$	~710°–~1200°C	~630°–~1260°C	Low-temperature, two-phase region
$\gamma + \delta$	~1200°–~1310°C	~1260°–~1390°C	Single-phase austenite region
$\delta$	~1310°–~1440°C	~1390°–~1440°C	High-temperature, two-phase region
$\delta + \text{liq.}$	~1440°–~1470°C	~1440°–~1470°C	Single-phase ferrite region
			Partially melted region

Table 2 — Steel Chemical Composition (wt-%)

Steel	C	Si	Mn	P	S	Cu	Ni	Cr	Mo	Al	N
A	0.020	0.28	0.18	0.015	0.0006	0.09	4.70	13.62	1.66	0.016	0.077
B	0.020	0.22	1.51	0.013	0.002	0.49	0.80	10.94	—	0.023	0.0092
C	0.11	0.15	0.54	0.006	0.001	0.15	0.49	13.10	—	0.003 <sup>(a)</sup>	0.066
D	0.028	0.30	0.49	0.012	0.001	1.43	3.76	11.16	1.17	0.020	0.0082
E	0.010	0.30	0.44	0.016	0.001	—	6.11	11.99	2.47	—	—

(a) Reported as soluble Al.

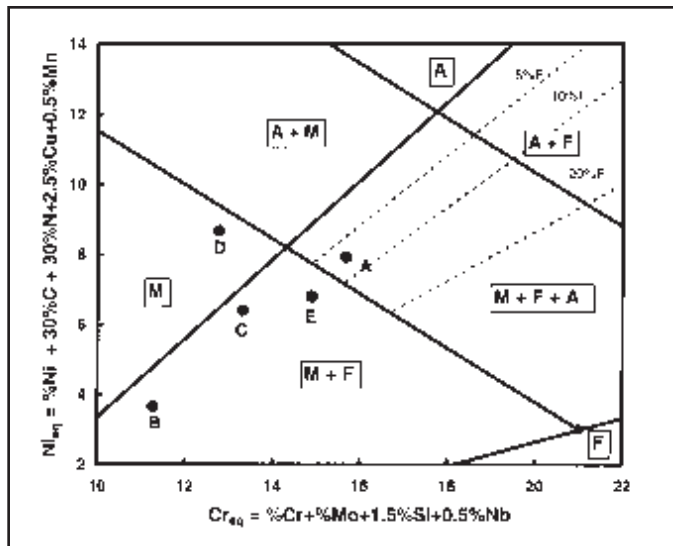


Fig. 2 — Schaeffler diagram, location of the investigated steels.

Table 3 — Base Metal Mechanical Properties

Steel	Yield Strength R <sub>p0.2</sub> (MPa)	Tensile Strength R <sub>m</sub> (MPa)	Elongation at Fracture (%)	Hardness (kg/mm <sup>2</sup> )
A	619–762	915–939	33	296
B	545	641	—	207
C	582–659	711–786	22.3	259
D	614	821	—	265
E	563–613	892–902	28	290

Table 4 — Microstructures<sup>(a)</sup> of Weld Simulated Specimens

Steel	Weld Thermal Cycle		
	T <sub>p</sub> = 1350°C	T <sub>p</sub> = 1000°C	T <sub>p</sub> = 800°C
A	M + F	Fine new M + F stringers + C (M <sub>23</sub> C <sub>6</sub> )	Fine-tempered M + F stringers + C (M <sub>23</sub> C <sub>6</sub> ) [similar to the base metal microstructure]
B	Coarse M + F	Fine new M + F retained grain boundary C	Fine-retained tempered M + new M [finer than the base metal microstructure]
C	M + F	Fine new M + F + retained C (M <sub>23</sub> C <sub>6</sub> )	Coarse-tempered M [similar to the base metal]
D	M + F (+ TiN)	Fine new M + F + tempered M + retained C (M <sub>23</sub> C <sub>6</sub> )	Coarse-tempered M [similar to the base metal]
E	M + F (+ TiN)	Fine new M + tempered M + retained C (M <sub>23</sub> C <sub>6</sub> ) + F stringers	Tempered M + F stringers [similar to the base metal], grain boundary C dissolved partially

(a) M = martensite, F = ferrite, C = carbides

### Testing and Characterization

All weld thermal simulated specimens were machined down to either the standard 10 × 10 × 55-mm Charpy V-notch dimensions for resistance-heated specimens or selected dimensions of tensile test specimens for induction-heated specimens prior to testing, i.e., L<sub>0</sub> = 35 mm, d = 5

mm. The CVN test temperature was 0°C. Tensile testing was carried out with a constant crosshead speed of 2 mm/min.

Standard metallography techniques were used in the preparation of specimens for microstructure characterization, using Vilella's reagent for etching. Hardness measurements were carried out with a 5-kg load (HV<sub>5</sub>).

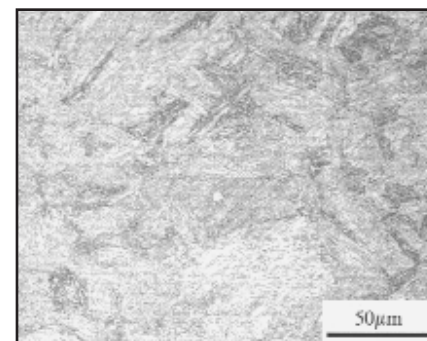
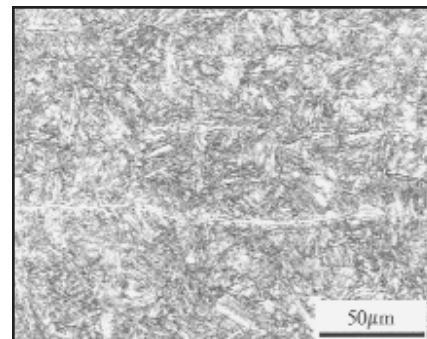


Fig. 3 — Base metal microstructures, steels A (above) and D (below).

## Results and Discussion

### Transformation Behavior

In general, it is seen from Fig. 4 that the transformation temperature decreases with an increase in the peak temperature. This observation is not surprising, since an increase in the peak temperature normally causes austenite grain growth and, hence, a certain hardenability increase (reduction of M<sub>s</sub>). The fact that M<sub>s</sub> is reduced with increasing peak temperature is partly a kinetic effect due to smaller grain boundary area available for nucleation, and partly a compositional effect since precipitated chromium carbides, M<sub>23</sub>C<sub>6</sub>, will dissolve at the highest temperatures and provide more carbon and alloying elements in solution. In the case of steels A and E, substantial scatter in the transformation temperatures was recorded. This was probably caused by the large variations in base metal microstructure, i.e., austenite grain size varies significantly. Apparently, the cooling time, Δt<sub>8/5</sub>, appears to have only a small effect on the transformation behavior.

It is also seen in Fig. 4 that the transformation behavior of the steels under examination was quite different. The recorded M<sub>s</sub> temperatures of steel A are below about 210°C for all thermal programs. The transformation temperatures of steel E were between 200° and 300°C, which is higher than that of steel A. The M<sub>s</sub> level is higher for steels C and D, which

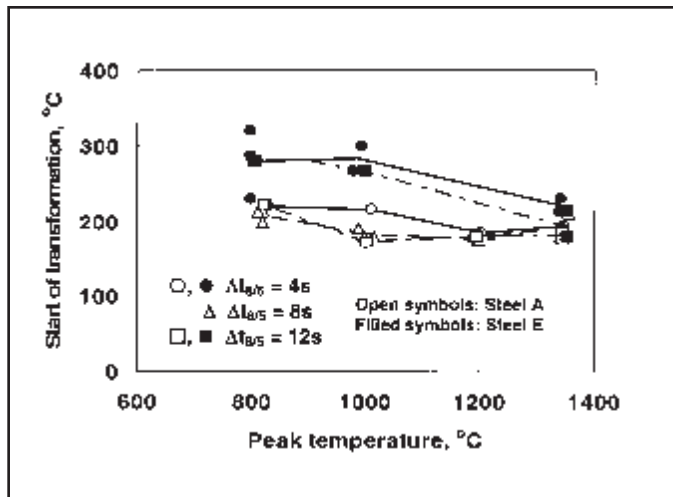


Fig. 4 — Transformation temperatures, steels A and E.

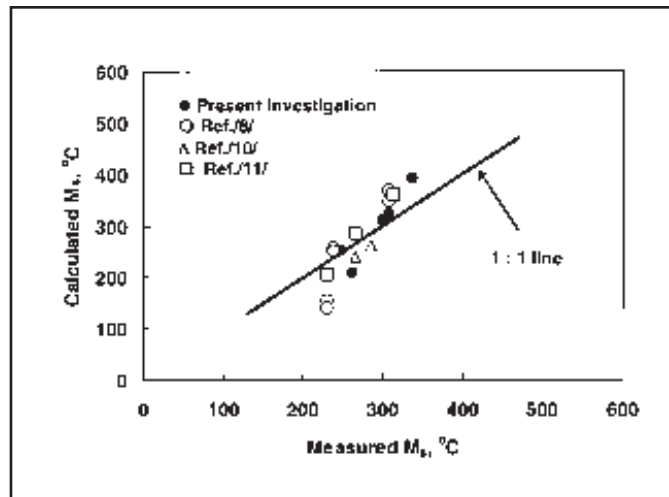


Fig. 5 — Comparison between calculated and measured temperature for start of martensite transformation,  $M_s$ . Mean values are used for steels A, B, C, D, and E.

show  $M_s$  temperatures between about 360° and 300°C. Steel B has the highest  $M_s$  temperatures (between 390° and 420°C, depending on the peak temperature), probably due to the lower alloying content of this steel. Thus, the transformation behavior of the steels reflects their respective alloying level. The high alloyed grades will have low  $M_s$  levels, say below 220°C, while medium grades will transform to martensite between 250 and 300°C. Finally, the lean grade will have  $M_s$  values above 300°C.

The transformation temperature  $M_s$  is very important, since it may strongly influence the evolution of residual stresses and strains, as well as the hydrogen transport and distribution during and after welding. Moreover, it strongly influences the selection of interpass temperature; the interpass temperature should be below  $M_s$  to ensure that all weld beads transform to martensite before the next bead is deposited, allowing tempering effects in multipass welding. It is, therefore, of interest to be able to predict the  $M_s$  temperature. In the literature, there are several empirical equations published to calculate the  $M_s$  value. According to Ref. 9, the best fit was obtained with the Andrews equation (quoted in Ref. 10). This equation is as follows:

$$M_s (°C) = 539 - 423 (\%C) - 30.4 (\%Mn) - 12.1 (\%Cr) - 17.7 (\%Ni) - 7.5 (\%Mo) \quad (1)$$

The correlation between measured and calculated values, using Equation 1 and the data in Table 2, is shown by the plot in Fig. 5. It is shown that the correlation is quite good, although the data imply that the  $M_s$  temperature is underestimated at low temperatures and overesti-

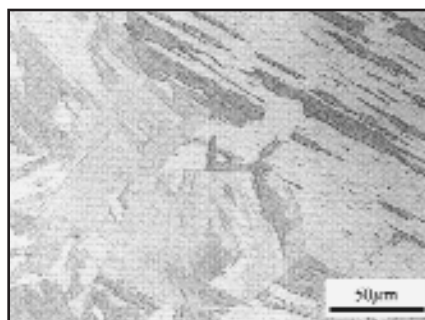


Fig. 6 — Grain-coarsened HAZ ( $T_p = 1350°C$ ) microstructure, steel B.

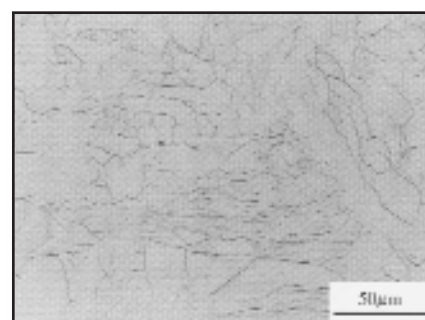


Fig. 7 — Grain-coarsened HAZ ( $T_p = 1350°C$ ) microstructure, steel A.

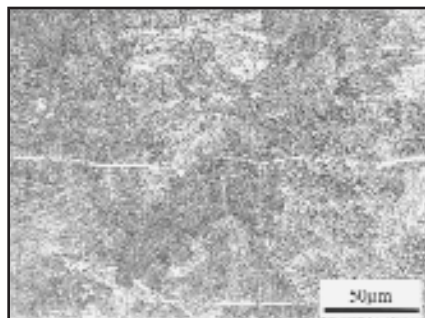


Fig. 8 — Grain-refined HAZ ( $T_p = 1000°C$ ) microstructure of steel E.

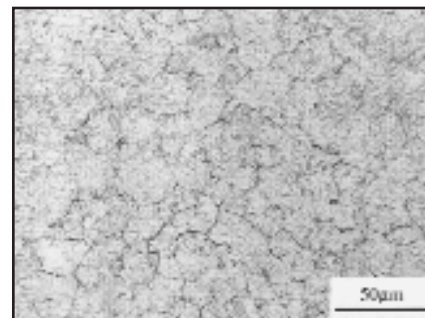


Fig. 9 — Microstructure of steel C after tempering at 800°C for 1 h ( $T_p = 1350°C/\Delta t_{8/5} = 5$  s).

ated at higher transformation temperatures. This is not necessarily due to an insufficient accuracy in the calculation, but also due to a wide scatter in measurements of the  $M_s$ .

When considering the end of transformation, the  $M_f$  point was found to be on average about 130°C below  $M_s$ :

$$M_f (°C) = M_s - 130 \quad (2)$$

This is not far from the 120°C, which is reported for low-carbon microalloyed and

low-alloy steel (Ref. 12). However, the difference between  $M_s$  and  $M_f$  seems to vary between 120° and 150°C when comparison is made with published CCT diagrams with a much lower austenitization temperature than used here (Ref. 8).

### Microstructure Characterization

Weld Simulation with Peak Temperature of 1350° and 1200°C

Inspections of the grain-coarsened HAZ (1350°C) microstructures shown in

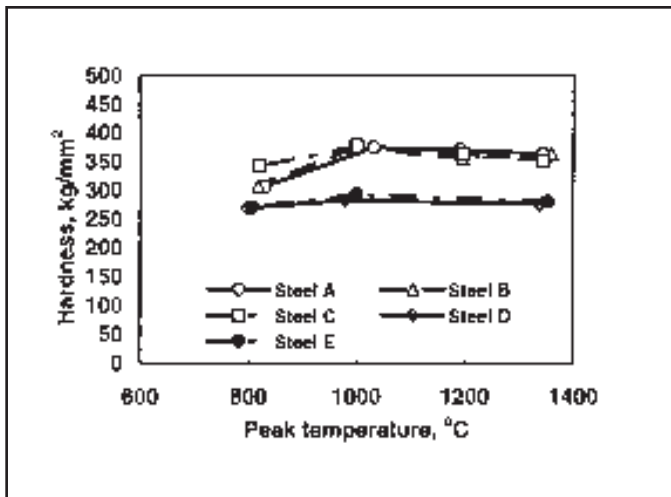


Fig. 10 — Effect of peak temperature on hardness.

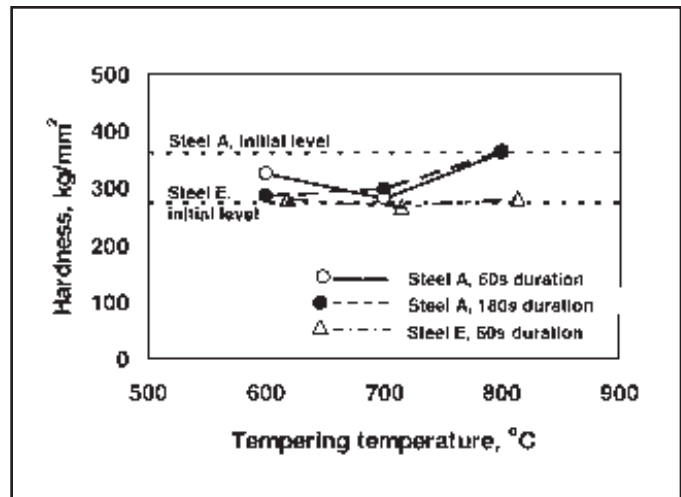


Fig. 11 — Effect of tempering temperature on hardness, steels A and E.

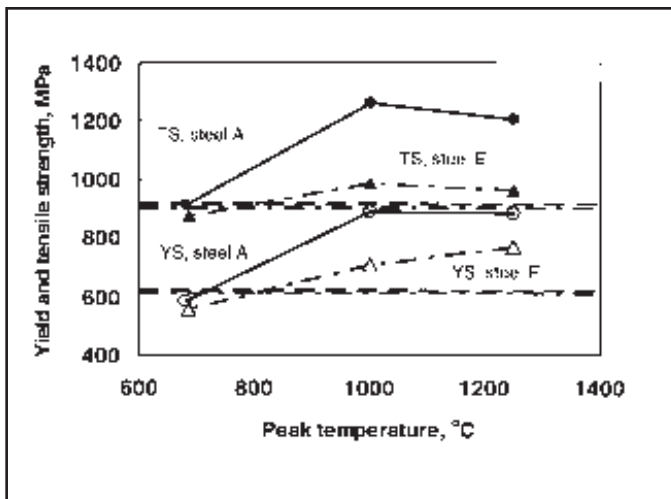


Fig. 12 — Effect of peak temperature on strength, steels A and E.

Figs. 6 and 7 reveal that they can be divided into two main categories: 1) coarse martensite within large prior austenite grains for the low-nickel-containing steels B, C, and D (Fig. 6); and 2) finer network of martensite with ferrite aligned at prior austenite grain boundaries in steels A and E — Fig. 7. These results may imply that the peak temperature of 1350°C for the two latter steels falls within the  $\alpha + \gamma$  region ( $\alpha$  = ferrite,  $\gamma$  = austenite), where  $\gamma$  transforms to martensite on cooling. At the peak temperature, the presence of the two phases tends to inhibit grain growth. There is small evidence of ferrite in steel B, also; some ferrite areas were observed in the base metal in the form of retained initial ferrite stringers. Apparently, the cooling time  $\Delta t_{8/5}$  did not affect the microstructure systematically; the small differences observed are probably caused by local material inhomogeneities and insufficient regulation during weld simulation

(occasional local melting). Still, the amount of ferrite in steel A seems to decrease with slower cooling rates. The microscopic observations are also summarized in Table 4.

As stated above, a peak temperature of 1350°C may fall within the  $\alpha + \gamma$  two-phase region, depending on the steel chemical composition. The austenite formed at the peak temperature will transform to martensite on

cooling, but usually with a much coarser lath structure than that of the base metal due to the large austenite grain size. By contrast, the ferrite will be stable down to ambient temperature. This observation is in agreement with recently published results (Ref. 13). Ferrite was not observed in steels B and C, which is in agreement with the low chromium equivalent values. However, it should be noted that steel D, which falls within the single-phase martensite region, contains substantial amount of ferrite after weld simulation, and its position in the Schaeffler diagram in Fig. 2 should be moved downward toward the border between M+F and M+F+A. The Schaeffler diagram should, therefore, be used with care for these steels, at least as far as the HAZ transformation behavior is concerned.

Few specimens were subjected to a peak temperature of 1200°C. This will be very close to full austenitization for all

steels. In the case of steel A, the austenite grain size increased considerably when the cooling time  $\Delta t_{8/5}$  increased from 4 to 12 s. On cooling, both martensite and ferrite formed.

#### Weld Simulation with Peak Temperature of 1000°C

With a peak temperature of 1000°C one may expect that the specimens were heated to the single-phase  $\gamma$  regime. The austenite formed will transform to martensite on cooling, but usually with a finer lath structure than that of the base metal. The presence of any undissolved chromium carbides may locally reduce the chromium equivalent value, and thus extend the austenite area. This may explain why the amount of ferrite was apparently reduced compared with the 1350°C cycle. However, nontransformed ferrite stringers were found, as shown by Fig. 8 (steel E).

#### Weld Simulation with Peak Temperature of 800° and 650°C

In general, the microstructures formed at 800°C are similar to those of the respective base metals, but with certain refinement. Although the  $A_{c1}$  temperature is not determined for steels A, D, and E, indications are that a small refinement of the initial base metal microstructure has occurred, which means that a small fraction has been austenitized during heating with subsequent martensite formation on cooling. A further evidence of this point would require scanning electron microscopy to obtain the necessary magnification to identify the small martensite islands. The refinement of the base metal microstructure is relatively clear in the case of steel B, and is in agreement with the increased hardness level (increased

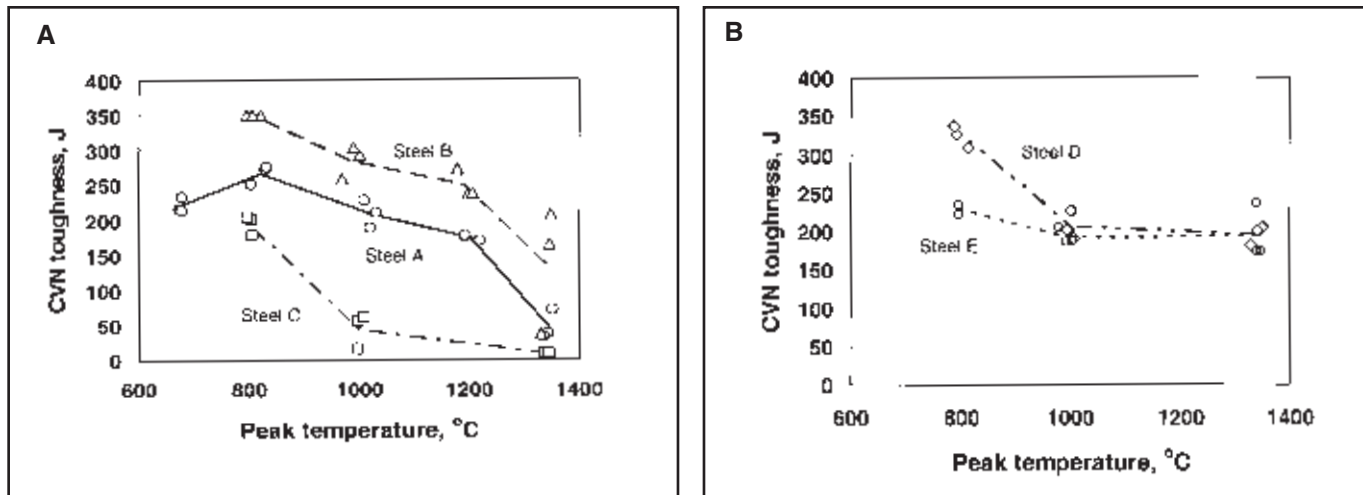


Fig. 13 — Effect of peak temperature on CVN toughness at 0°C;  $\Delta t_{8/5} = 5$  s. A — Steel A, B, and C; B — steels D and E.

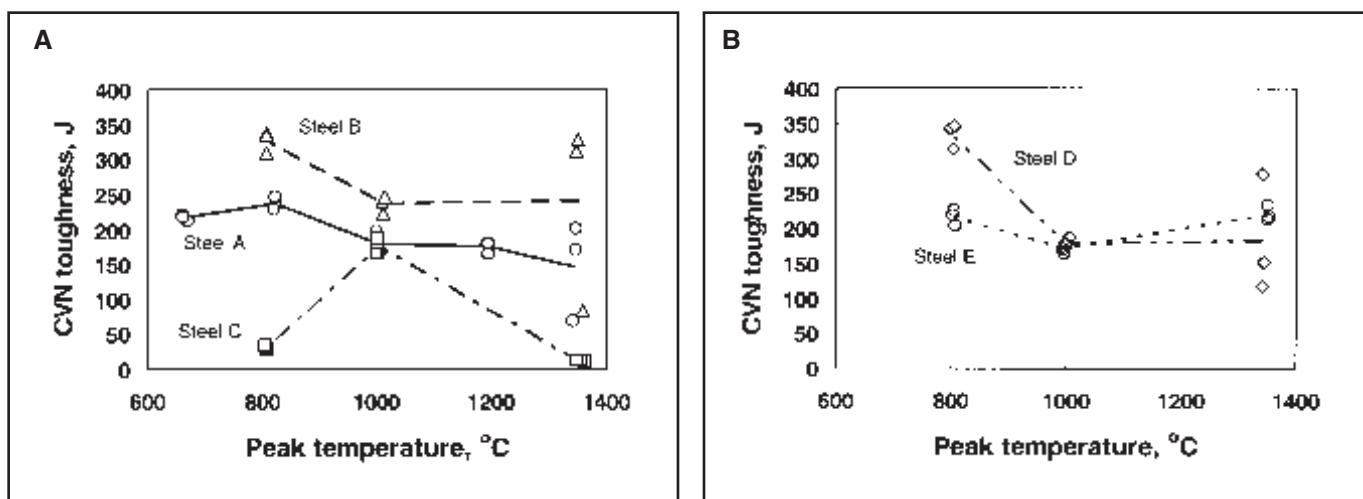


Fig. 14 — Effect of peak temperature on CVN toughness at 0°C;  $\Delta t_{8/5} = 12$  s. A — Steels A, B, and C; B — steels D and E.

from 207 to 252–262 HV). A similar hardness increase has been found for steel A (increase from 289 to 306–341 HV). By contrast, the base metal hardness is reduced after simulation for the other steels. It is reasonable to suggest that this observation is due to a stronger softening effect by tempering than a hardness increase from new martensite formation.

In the case of steel A, when using peak temperature of 650°C, the microstructure appeared to be very similar to that of the base metal. No visible effect of the cooling rate was found.

#### Weld Simulation with Subsequent Tempering Pulses at 600°, 700°, and 800°C

In contrast to the previous weld simulation experiments, with the base plate microstructure as a basis for discussion, the initial microstructure for the tempering

pulses is the one formed under single cycle with peak temperature  $T_p$  of 1350°C (left column in Table 4). For the high-Ni-containing steels A, D, and E, the microstructure after tempering at 600°C consisted of tempered martensite with some ferrite. Steel C showed tempered martensite with extensive bulk and grain boundary carbide precipitation due to its high carbon content. At 700°C, however, the carbides were mainly found at grain boundaries for all steels. Steel B appeared to be relatively resistant to tempering, and its response to chemical etching is much more sluggish than that of the other steels. For a peak temperature of 700°C, it is possible to see that some austenitization has taken place with some new formation of martensite with nontransformed residual austenite. At 800°C, an even larger fraction has been retransformed. The reformation of martensite was confirmed by the hardness

increase for steels A, B, C, and E when increasing the tempering temperature from 700° to 800°C. This observation can be seen in the micrograph in Fig. 9, revealing also grain boundary phases (martensite/retained austenite and  $M_{23}C_6$ ) in steel C.

#### Hardness

The hardness (HV<sub>5</sub>, 5-kg load) values have been plotted against the peak temperature in Fig. 10. It can be seen from the figure that the hardness level is relatively similar for all peak temperatures, which also would be expected if the microstructure was fully martensitic with a low  $M_s$  temperature, i.e., with negligible autotempering during cooling. An exception is found for a peak temperature of 800°C for steels A, B, and, partly, C, where the hardness level has been significantly reduced.

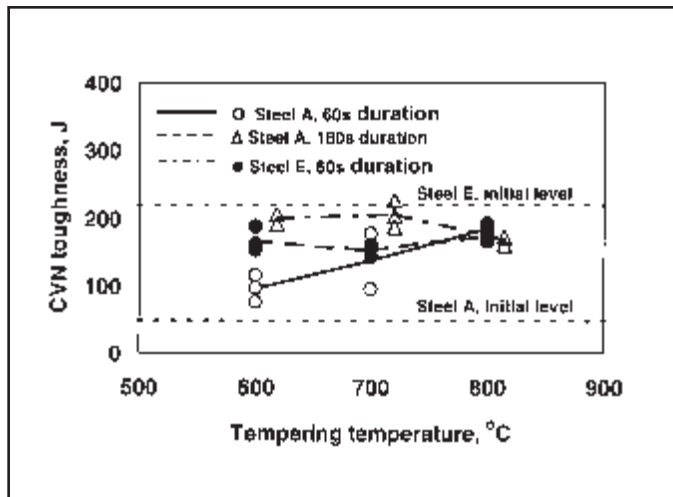


Fig. 15 — Effect of tempering temperature on CVN toughness at 0°C, steels A and E.

It is reasonable to suggest that this observation is linked to a stronger hardness reduction effect of tempering than hardness increase as a consequence of reaustenitization with subsequent formation of new martensite on cooling.

The hardness level was in general reduced by the following tempering pulses, particularly for steel C where the initial level after the 1350°C cycle (shown as the dashed line in Fig. 11 for all steels) was very high. An exception is found for the tempering pulse carried out at 800°C. In this case, the initial hardness level is restored for all steels except for steel C. Data for steel A may imply that the tempering time has only marginal influence on hardness, but the effect is larger at lower tempering temperatures.

#### Strength and Ductility

The data from tensile testing of weld simulated (induction heated) specimens are shown in Fig. 12. Here, the base metal yield and tensile strength levels are also included for comparison. It is seen from the figure that both yield and tensile strength levels have been substantially increased for the highest peak temperatures of 1250° and 1000°C, which is also expected since the new martensite is not subjected to tempering during cooling from the peak temperature. At the lowest peak temperature (680°C), only tempering is expected to occur, and the slight reduction in yield strength in this case is therefore not surprising. These trends were observed for all steels (exemplified by steels A and E in Fig. 12), with exception of steel C, where the strength level was similar to the initial base metal strength, independent of the peak temperature, i.e., yield and tensile strength level of 620–660 MPa and 780–800 MPa, re-

spectively. The highest HAZ strength was found for steel A, represented by the values of 887 and 1260 MPa for yield and tensile strength, respectively.

For all steels, the initial base metal elongation at fracture appeared to be slightly reduced with peak temperatures of 1000° and 1250°C, while they were unchanged at the lowest temperature of 650°C. In the case of the reduction in area, a very small reduction was found for steels A, B, and D, while a negligible increase was seen for the two other steels C and E.

#### CVN Toughness

In general, the CVN toughness at 0°C of weld simulated (resistance heated) specimens were relatively high, as shown by Figs. 13 and 14 for a cooling time  $\Delta t_{8/5}$  of 5 and 12 s, respectively. An exception is low values observed for the 1350°C cycle for steel C, and occasionally also for steels A and B. The data in Fig. 13 showed typically a CVN toughness deterioration with increasing peak temperatures, which is possibly related to the finer microstructure, as discussed previously.

In the case of subsequent tempering heat treatment, the steels responded quite differently. Here, steel A was the only one where tempering gave rise to a notch toughness enhancement for all temperatures employed. The results for steel A are shown in Fig. 15. Included in the figure are data for steel E, which showed an opposite trend, i.e., tempering deteriorated impact toughness at all temperatures. However, the toughness of this steel is still higher than that of steel A, with an exception of tempering at 800°C.

Steels B, C, and D were susceptible to embrittlement. Steel B appeared with low toughness at 700°C, which means an average impact strength of 28 J. Steel C had very low values for both 600°C (< 10 J) and 800°C (25 J average). Finally, steel D had low toughness at 600°C (14 J average), with large scatter at 700°C (three parallels of 17, 30, and 218 J).

It is very difficult to explain this different behavior of the examined steels. Various mechanisms are probably involved, possibly

ranging from temper embrittlement by impurity element segregation (e.g., phosphorus), new formation of nontempered martensite, or islands of stable austenite. A clarification of the mechanisms involved will be important in further work on these steels, since it may influence their behavior during fabrication and subsequent service.

#### Implications of the Present Work

The present investigation has been a part of a large qualification program of 13% Cr martensitic stainless steels for applications in offshore flowline and risers, where extensive corrosion testing and welding experiments have been included (e.g., Refs. 14–20). The results obtained show that the “old, traditional” 13% Cr steels (steel C) contain too high carbon content, which gives a very high hardness level of about 500 kg/mm<sup>2</sup>. This is far beyond an acceptable level, even after tempering. With a hard martensite present, the steel will be very susceptible to hydrogen cracking, and expensive operations like preheating and postheating may be necessary, as well as certain precautions regarding welding consumables and shielding gas moisture must be taken. In addition to the very high hardness, steel C was the only one with low CVN impact values (< 50 J) in the as-weld-simulated condition. After tempering, only the high-alloy steel E (12Cr-6Ni-2.5Mo) and the lean alloy steel A (13Cr-4.7Ni-1.7Mo), both with low carbon (< 0.02% C) content, revealed good toughness (between 100 and 200 J). The compositions of these steels are very close to those now commercially available.

Note that the short pulse tempering is used since long-time postweld heat treatment is not possible in the present application.

#### Conclusions

Based on the present investigation the following main conclusions can be drawn:

- The heat-affected zone hardness level is strongly dependent on the steel's chemical composition and the weld thermal program. A relatively low hardness (270–290 kg/mm<sup>2</sup>) can be obtained for the low-carbon (0.01–0.02 wt-% C) steels B and E even in the as-weld-simulated condition. Steels A, C, and D showed values beyond 300 kg/mm<sup>2</sup>, possibly due to high carbon (steels C and D) and high chromium content (steel A).
- The hardness levels are reduced by subsequent tempering pulses.
- In general, the Charpy V-notch toughness was high (> 200 J), with exception of the very high carbon-containing steel C and some low values for steels

A and B for a peak temperature of 1350°C. The CVN level varies with the applied peak temperature, with less influence of the cooling time  $\Delta t_{8/5}$  (comparison between Figs. 13 and 14).

- The effect of subsequent tempering pulses is dependent on the initial CVN toughness after the first weld cycle of  $T_p \sim 1350^\circ\text{C}$ .

### Acknowledgments

The authors wish to thank Statoil for its financial contribution, and Ms. Solveig Kirknes for performing the weld simulation experiments.

### References

1. Enerhaug, J., Eliassen, S. L., and Kvaale, P. E. 1997. *Proc. Corrosion '97*, paper no. 60, p. 28. Houston, Tex.: NACE International.
2. Enerhaug, J., Kvaale, P. E., Bjordal, M., Drugli, J. M., and Rogne, T. 1999. *Proc. Corrosion '99*, paper no. 587, p. 13. Houston, Tex.: NACE International.
3. Olsen, S., Kvaale, P. E., and Enerhaug, J. 1999. *Proc. Supermartensitic Stainless Steels '99*, Brussels, Belgium, pp. 84–87. Belgian Welding Institute.
4. Folkhard, E. 1988. *Welding Metallurgy of Stainless Steels*. Springer Verlag.

5. Enerhaug, J., Grong, Ø., and Steinsmo, U. M. 2001. *Science and Technol. in Weld. and Join.* 6(5): 330–338.
6. Carrouge, D., and Woollin, P. 2002. *Stainless Steel World*, paper PO233, pp. 61–67.
7. Dufrane, J. J. 1999. *Proc. Supermartensitic Stainless Steels '99*, Brussels, Belgium, pp. 19–24. Belgian Welding Institute.
8. Toussaint, P., and Dufrane, J. J. 2002. *Proc. Supermartensitic Stainless Steels 2002*, Brussels, Belgium, pp. 23–27. Belgian Welding Institute.
9. Beres, L., Beres, Z., and Irmer, W. 1994. *Schweissen & Schneiden* 46(8): E128–E130.
10. Acevedo, D., Svoboda, H., Surian, E., Ramini de Rissone, N. M., and De Vedia, L. A. 1999. *Proc. Supermartensitic Stainless Steels '99*, Brussels, Belgium, pp. 101–108. Belgian Welding Institute.
11. Heuser, H., Jochum, C., Perteneder, E., and Tösch, J. 1999. *Proc. Supermartensitic Stainless Steels '99*, Brussels, Belgium, pp. 150–159. Belgian Welding Institute.
12. Akselsen, O. M., Grong, Ø., and Rørvik, G. 1990. *Scand. J. Met.* 19: 258–264.
13. Woollin, P., and Carrouge, D. 2002. *Proc. Supermartensitic Stainless Steels 2002*, Brussels, Belgium, pp. 199–204. Belgian Welding Institute.
14. Akselsen, O. M., Rørvik, G., van der Eijk, C., and Kvaale, P. E. 2000. *Proc. Nordic Welding Conference*, September 20–22, Iceland.
15. Rogne, T., and Svenning, M. 2002. *Proc. Supermartensitic Stainless Steels 2002*, Brussels, Belgium, pp. 178–184. Belgian Welding Institute.

16. Enerhaug, J., Wenn, T., Steinsmo, U. M., and Grong, Ø. 2002. *Proc. Supermartensitic Stainless Steels 2002*, Brussels, Belgium, pp. 185–193. Belgian Welding Institute.
17. Enerhaug, J., Steinsmo, U. M., Grong, Ø., and Hellevik, L. R. 2002. *J. Electrochem. Soc.*, 149(6): B256–B264.
18. Enerhaug, J. 2002. Ph.D. thesis. The Norwegian University of Science and Technology, Dept. of Machine Design and Materials Technology, Trondheim.
19. Aune, R., Fostervoll, H., Akselsen, and O. M. 2003. *Proc. Int. Conf. OMAE 2003 (the 22nd Int. Conf. on Offshore Mechanics and Arctic Engineering)*, Cancun, Mexico.
20. Aune, R., Fostervoll, H., Akselsen, and O. M. 2003. *Proc. Int. Conf. OMAE 2003 (the 22nd Int. Conf. on Offshore Mechanics and Arctic Engineering)*, Cancun, Mexico.

**HOTTEST WELDING BOOKS ON THE WEB**

[www.aws.org/catalogs](http://www.aws.org/catalogs)

## CAN WE TALK?

The *Welding Journal* staff encourages an exchange of ideas with you, our readers. If you'd like to ask a question, share an idea or voice an opinion, you can call, write, e-mail or fax. Staff e-mail addresses are listed below, along with a guide to help you interact with the right person.

### Publisher/Editor

Andrew Cullison  
[cullison@aws.org](mailto:cullison@aws.org), Extension 249  
 Article Submissions

### Senior Editor

Mary Ruth Johnsen  
[mjohnsen@aws.org](mailto:mjohnsen@aws.org), Extension 238  
 Feature Articles

### Associate Editor

Howard Woodward  
[campbell@aws.org](mailto:campbell@aws.org), Extension 244  
 Society News  
 Personnel

### Associate Editor

Ross Hancock  
[rhancock@aws.org](mailto:rhancock@aws.org), Extension 226  
 New Products  
 New Literature

### Production Editor

Zaida Chavez  
[zaida@aws.org](mailto:zaida@aws.org), Extension 265  
 Design and Production

### Advertising Sales Director

Rob Saltzstein  
[salty@aws.org](mailto:salty@aws.org), Extension 243  
 Advertising Sales

### Advertising Production Coordinator

Frank Wilson  
[fwilson@aws.org](mailto:fwilson@aws.org); Extension 465  
 Advertising Production

### Advertising Sales & Promotion Coordinator

Lea Garrigan  
[garrigan@aws.org](mailto:garrigan@aws.org), Extension 220  
 Production and Promotion

### Peer Review Coordinator

Doreen Kubish  
[doreen@aws.org](mailto:doreen@aws.org), Extension 275  
 Peer Review of Research Papers

Welding Journal Dept.  
 550 N.W. LeJeune Rd.  
 Miami, FL 33126  
 (800) 443-9353  
 FAX (305) 443-7404